

Superconductivity near an Ising nematic quantum critical point in two dimensions

Jie Huang,¹ Zhao-Kun Yang,¹ Jing-Rong Wang,² and Guo-Zhu Liu^{1,*}

¹*Department of Modern Physics, University of Science and Technology of China, Hefei, Anhui 230026, China*

²*High Magnetic Field Laboratory of Anhui Province,
Chinese Academy of Sciences, Hefei 230031, China*

Near a two-dimensional Ising-type nematic quantum critical point, the quantum fluctuations of the nematic order parameter are coupled to the electrons, leading to non-Fermi liquid behavior and unconventional superconductivity. The interplay between these two effects has been extensively studied through the Eliashberg equations for the superconducting gap. However, previous studies often rely on various approximations that may introduce uncertainties in the results. Here, we revisit the issue of how the superconducting transition temperature T_c is affected by removing certain common approximations. We numerically solve the self-consistent Dyson-Schwinger equations of the electron propagator $G(p)$, the nematic propagator $D(q)$, and the vertex function $\Gamma_v^{1L}(p+q,p)$ expanded up to the triangle order, without introducing further approximations. Our calculations reveal that the extended s -wave superconducting gap is the only convergent solution to the nonlinear gap equations. We investigate the evolution of T_c as the system approaches the nematic quantum critical point from the disordered (tetragonal) phase. Under the bare vertex approximation, T_c is monotonically enhanced. However, when vertex corrections are incorporated, T_c initially increases but then decreases, with the maximum value of T_c occurring at a point away from the quantum critical point. The obtained gap symmetry and the non-monotonic behavior of T_c are compared with recent experiments on doped FeSe materials.

I. INTRODUCTION

The electronic nematic order refers to a state of quantum matter that spontaneously breaks the C_4 -symmetry down to a C_2 -symmetry. Investigations of this order date back to Kivelson, Fradkin, and Emery¹, who predicted the existence of electronic nematicity in normal states of cuprate superconductors as a result of the stripe melting. Formation of electronic nematic order can also be studied from a different perspective^{2,3}, namely the Pomeranchuk instability of the Fermi surface. When a system exhibits nematic order, its resistivity and other observable quantities become strongly anisotropic. Experimentally, clear signatures of electronic nematic order have been observed in many condensed matter systems, including cuprates^{4–14}, iron-based superconductors^{15–43}, some heavy-fermion superconductor⁴⁴, Sr_2RuO_4 ⁴⁵, Kagome superconductors^{46–48}, magic-angle graphene^{49,50}, superconducting nickelate⁵¹, and $\text{Ba}_{1-x}\text{Sr}_x\text{Ni}_2\text{As}_2$ ⁵². Many of these superconductors share two common features: the presence of a dome shape for the superconducting transition temperature T_c and the emergence of non-Fermi liquid (NFL) behavior in the normal state.

In iron-based superconductors, the electronic nematic order almost always coexists with antiferromagnetism or charge-density-wave order, making it hard to disentangle the intrinsic effect of the electronic nematicity on superconductivity. FeSe ^{18,19,28–43} has attracted special interest because this material displays nematic order but is not magnetically ordered. At ambient pressure, FeSe undergoes a nematic transition at the critical temperature $T_s \approx 90$ K without any long-range magnetic order. Chemical substitution of Se by S or Te tunes T_s down to zero, yielding a well-defined nematic quantum critical point (QCP) at $x_c = 0.17$ in $\text{FeSe}_{1-x}\text{S}_x$ and at $x_c = 0.50$

in $\text{FeSe}_{1-x}\text{Te}_x$. Nematic QCP can also be realized when the pressure^{30,34,41} applied to $\text{FeSe}_{1-x}\text{S}_x$ exceeds certain threshold p_c . These nematic QCPs provide an ideal platform for exploring the exclusive impact of the nematic quantum criticality on both superconductivity and NFL behavior.

Now consider the nematic QCP defined at a critical non-thermal parameter $x = x_c$. Without loss of generality, the system is supposed to be tetragonal for $x > x_c$ and orthohombic for $x < x_c$. While the nematic order parameter has a vanishing vacuum expectation value ($\langle \phi \rangle = 0$) at the QCP, nematic quantum fluctuations are significant and interact strongly with gapless electrons near the Fermi surface. This interaction can be modeled by a Yukawa-type fermion-boson coupling. The physical effects of this coupling have been studied for decades by employing various analytical and numerical techniques^{2,3,53–74}. Many of these calculations predicted that this coupling induces NFL behavior at high temperatures and unconventional superconductivity at low temperatures under appropriate conditions. Especially, the superconductivity mediated by nematic fluctuations was found to be significantly enhanced at the nematic QCP and suppressed as the system is tuned away from the QCP^{56–59,63,64}, implying that optimal superconductivity is realized right at the nematic QCP. These results are anticipated to offer a promising explanation for the two aforementioned common features of unconventional superconductors.

However, recent experiments have provided only limited support for the theoretical predictions mentioned above. The evolution of T_c across the nematic QCPs is not universal, but material dependent. In $\text{FeSe}_{1-x}\text{S}_x$, T_c is hardly modified as the system is tuned across the QCP. For $\text{FeSe}_{1-x}\text{Te}_x$, although a superconducting dome

was observed near the nematic QCP^{36,37,39}, the value of T_c is not maximized exactly at the QCP. There is not a well-established explanation for such an anomalous dependence of T_c on the distance to nematic QCP.

In this paper, we revisit the quantum criticality of an Ising-type nematic transition in two spatial dimensions and study the properties of the superconductivity that emerges from the NFL state near the nematic QCP. The nematic order is assumed to have a d -wave symmetry, characterized by an anisotropic form factor in the Yukawa coupling term^{58,68}. For simplicity, we only consider the disordered side of nematic transition, where $x \geq x_c$. In the limits of $x \gg x_c$ and $x \rightarrow x_c$, the system behaves as a normal FL and a typical NFL, respectively. Within the broad intermediate range of x , the system resides in a mixed FL/NFL regime, exhibiting FL behavior at low energies and NFL behavior at high energies.

NFL behavior and superconductivity are both induced by the same Yukawa coupling, implying that they can mutually influence each other. Consequently, they should be treated on an equal footing. In some previous theoretical works^{58,62,66,68–70,73,74}, their interplay has been studied using the Migdal-Eliashberg (ME) theory^{75,76}, which neglects all the vertex corrections to the Yukawa coupling. From a technical perspective, solving the self-consistent ME equations for renormalization factors and pairing function is challenging because they are highly nonlinear and have several variables. To reduce computational difficulty, a series of approximations have been introduced in practical computations. For instance, the nonlinear equations are often linearized in the vicinity of T_c . The boson self-energy, also called polarization function, is typically computed perturbatively under random phase approximation (RPA). Moreover, the electron momentum is usually restricted to the Fermi surface. While these approximations substantially simplify the original nonlinear equations, they may discard subtle feedback between NFL behavior and Cooper pairing and therefore lead to uncertainties in the predicted value of T_c .

Here, we study the superconducting pairing mediated by nematic quantum fluctuations by incorporating the vertex corrections into the ME theory. To describe NFL behavior and Cooper pairing equally, we employ the self-consistent Dyson-Schwinger (DS) equations satisfied by the renormalized electron propagator $G(p)$, the renormalized nematic propagator $D(q)$, and the vertex function $\Gamma^{1L}(p+q, p)$ that includes the contribution of the lowest order vertex corrections. We convert these DS equations to four nonlinear integral equations for the wave-function renormalization $A_1(p)$, the mass renormalization factor $A_2(p)$, the pairing function $\Phi(p)$, and the boson polarization $\Pi(q)$. These equations fully capture the mutual influence of various quantum critical phenomena, such as Landau damping, electron mass renormalization, and superconducting pairing. We then solve these equations numerically in a self-consistent manner, without adopting linearization and Fermi-surface approximation. Our

numerical calculations show that extended s -wave gap is the only stable convergent solution of the nonlinear equations. Strikingly, we find that the inclusion of vertex corrections can qualitatively change the behavior of T_c . Within the bare-vertex approximation, T_c is enhanced monotonously as the QCP is approached. After including vertex corrections, T_c exhibits a non-monotonic dependence on the boson mass parameter r that measures the distance of the system to nematic QCP where $r = 0$: T_c first increases and then decreases as r is lowering. We demonstrate that the non-monotonicity of T_c originates from a complicated interplay between NFL behavior and Cooper pairing. This theoretical result provides a possible explanation of the non-monotonic doping dependence of T_c observed in the tetragonal phase of $\text{FeSe}_{1-x}\text{Te}_x$ superconductor^{36,37,39}.

The rest of the paper is arranged as follows. In Sec. II, we define the effective model of nematic quantum critical systems and obtain the self-consistent DS integral equations for $A_1(p)$, $A_2(p)$, $\Phi(p)$, and $\Pi(q)$. In Sec. III, we present the numerical solutions of these equations and then analyze their physical implications. The theoretical results are compared with experiments on FeSe family superconductors. In Sec. IV, we briefly summarize the results and highlight further projects.

II. EFFECTIVE MODEL

We consider a $(2+1)$ -dimensional field theory that describes the interaction between the gapless electrons and the nematic quantum fluctuations, which is expressed as

$$\mathcal{L} = \psi^\dagger(i\epsilon_n - \xi_{\mathbf{p}})\psi - g\hat{f}(\mathbf{p})\phi\psi^\dagger\psi + \phi^\dagger((i\omega_m)^2/v_B^2 - \mathbf{q}^2 - r)\phi, \quad (1)$$

where ψ and ϕ are the field operators of electrons and nematic fluctuations, respectively. Within the Matsubara formalism, for notational simplicity, the electron and boson energy-momenta are denoted by $p = (i\epsilon_n, \mathbf{p})$ and $q = (i\omega_m, \mathbf{q})$, respectively. The electron frequencies are $\epsilon_n = (2n+1)\pi T$ and the boson frequencies are $\omega_m = 2m\pi T$. The electron dispersion is $\xi_{\mathbf{p}} = \frac{\mathbf{p}^2}{2m} - E_F$, where E_F is the Fermi energy. The boson mass r serves as the non-thermal parameter that tunes nematic quantum phase transition at zero temperature, with $r = 0$ marking the nematic QCP. Our current interest is restricted to the disordered side of nematic transition, corresponding to positive values of r . The precise value of boson velocity v_B is currently unknown. It is generally assumed⁷⁷ that v_B is of the same order of magnitude as the electron Fermi velocity v_F . For simplicity, we set $v_B = v_F$.

The boson self-coupling term $(\phi^\dagger\phi)^2$ is usually an irrelevant perturbation, especially near the QCP, and thus is not included. The effective strength of the Yukawa coupling is strongly anisotropic, characterized by a constant g and an angle-dependent form factor $\hat{f}(\mathbf{p})$. Following

the works of Lederer *et al.*⁵⁸ and Klein *et al.*^{68,69,72}, we consider the following *d*-wave form factor:

$$f(\mathbf{p}) = \frac{p_x^2 - p_y^2}{p_x^2 + p_y^2}. \quad (2)$$

Using the standard Nambu spinor⁷⁸, denoted by Ψ , and the Pauli matrices, we re-write the Lagrangian density as

$$\mathcal{L} = \Psi^\dagger (i\epsilon_n \sigma_0 - \xi_{\mathbf{p}} \sigma_3) \Psi - g f(\mathbf{p}) \phi \Psi^\dagger \sigma_0 \Psi + \phi^\dagger ((i\omega_m)^2 / v_B^2 - \mathbf{q}^2 - r) \phi. \quad (3)$$

The free electron propagator is

$$G_0(p) \equiv G_0(\epsilon_n, \mathbf{p}) = \frac{1}{i\epsilon_n \sigma_0 - \xi_{\mathbf{p}} \sigma_3}, \quad (4)$$

and the free boson propagator is

$$D_0(q) \equiv D_0(\omega_m, \mathbf{q}) = \frac{1}{(i\omega_m)^2 / v_B^2 - \mathbf{q}^2 - r}. \quad (5)$$

The free and fully renormalized electron propagators satisfy the following DS equation

$$G^{-1}(p) = G_0^{-1}(p) + g^2 \int_q f^2 \left(\mathbf{p} + \frac{\mathbf{q}}{2} \right) D(q) \times \sigma_3 G(p+q) \Gamma_v(p+q, p), \quad (6)$$

where $G(p)$ is the full electron propagator, $D(q)$ is the full boson propagator, and $\Gamma_v(p+q, p)$ is the the full vertex function. The abbreviation for integration measure is

$$\int_q \equiv \int \frac{d^3 q}{(2\pi)^3} = T \sum_m \int \frac{d^2 \mathbf{q}}{(2\pi)^2}. \quad (7)$$

The DS equation of the full boson propagator $D(q)$ has the form

$$D^{-1}(q) = D_0^{-1}(q) - \Pi(q), \quad (8)$$

where the polarization function is

$$\Pi(q) = g^2 \text{Tr} \int_p f^2 \left(\mathbf{p} + \frac{\mathbf{q}}{2} \right) \sigma_3 G(p) \Gamma_v(p+q, p) G(p+q), \quad (9)$$

where

$$\int_p \equiv \int \frac{d^3 p}{(2\pi)^3} = T \sum_n \int \frac{d^2 \mathbf{p}}{(2\pi)^2}. \quad (10)$$

The DS equations of $G(p)$ and $D(q)$ cannot be solved without a detailed knowledge of the vertex function $\Gamma_v(q, p)$. Currently, it is not possible to determine the exact form of $\Gamma_v(q, p)$. In the literature, a commonly adopted approach is to introduce the bare-vertex approximation, which amounts to setting $\Gamma_v(q, p) \rightarrow g\sigma_3$, even though there is no Migdal theorem ensuring the

smallness of vertex corrections. Under such a bare-vertex approximation, the DS equations of $G(p)$ and $D(q)$ become self-closed, leading to the well-known ME equations^{75,76}. The ME theory has achieved great success in the theoretical description of phonon mediated superconductivity in ordinary metals^{79–82}, and also has been applied to study unconventional superconductivity driven by the quantum fluctuations of various order parameters^{58,62,68–70,73,74,83,84}. The results obtained by solving ME equations are expected to be reliable if the vertex corrections are negligible.

For electron-phonon systems, the Migdal theorem⁷⁵ ensures that the vertex corrections are strongly suppressed by the small factor $\lambda\omega_D/E_F \leq 1$, where λ is a dimensionless coupling parameter and ω_D is Debye frequency. If the condition $\lambda\omega_D/E_F \leq 1$ is not fulfilled, vertex corrections may play a significant role and cannot be naively neglected. For instance, Esterlis *et al.* found a breakdown of ME theory⁸⁵ in a two-dimensional Holstein model with $\lambda > 0.4$. In some real superconductors, the Fermi energy E_F is quite small due to the extraordinarily low density of carriers. A notable example is SrTiO₃⁸⁶, where the ratio $\omega_D/E_F \gg 1$. In these superconductors, the ME formalism is believed to be invalid even though λ is small.

The effective model for nematic quantum criticality lacks a small parameter analogous to the ratio ω_D/E_F in electron-phonon systems. Thus, the vertex corrections are only negligible when the Yukawa coupling parameter g is sufficiently small. Nevertheless, in the absence of a satisfactory method of handling vertex corrections, the ME theory is still widely applied to study nematic quantum criticality. In addition to omitting vertex corrections, a couple of other approximations have been adopted to further simplify the complex ME equations.

The energy-momentum dependence of the polarization $\Pi(q)$ determines the effective strength of Yukawa coupling. Unfortunately, the concrete expression of $\Pi(q)$ can hardly be obtained. In earlier works, $\Pi(q)$ is usually computed within the perturbation theory. At the level of RPA^{55,58,62,68–70,73,74}, the one-loop polarization is given by

$$\Pi_1(q) = g^2 \text{Tr} \int \frac{d^3 k}{(2\pi)^3} f^2 \left(\mathbf{p} + \frac{\mathbf{q}}{2} \right) \sigma_3 G_0(k) \sigma_3 G_0(k+q), \quad (11)$$

which behaves as

$$\Pi_1(q) = -g^2 f^2 \left(\mathbf{p} + \frac{\mathbf{q}}{2} \right) \frac{|\omega_m|}{|\mathbf{q}|} \quad (12)$$

in the region $|\omega_m| \ll |\mathbf{q}|$. This polarization has a simple form and can be used to compute the one-loop electron self-energy $\Sigma(\epsilon_n, \mathbf{p})$ at zero temperature. At the Fermi momentum \mathbf{p}_F , the electron self-energy is found to display the following frequency dependence:

$$\Sigma_1(\epsilon_n) \propto |\epsilon_n|^{2/3}. \quad (13)$$

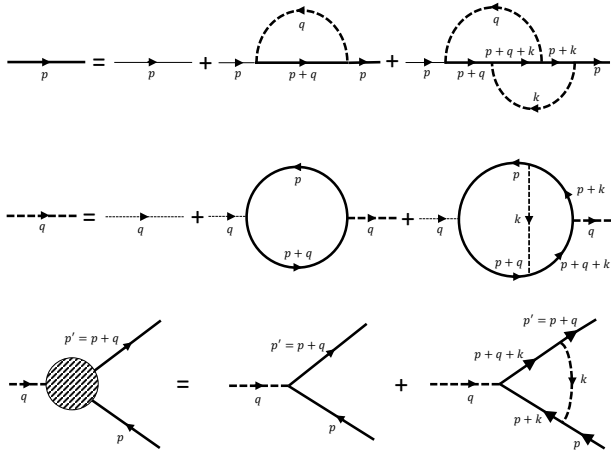


FIG. 1: Diagrams for the DS equations of $G(p)$, $D(q)$, and $\Gamma_v^1(p+q, p)$. Thin and thick solid (dashed) lines represent free and renormalized electron (boson) propagators, respectively.

The above expressions of $\Pi_1(q)$ and $\Sigma_1(\epsilon_n)$ are both obtained based on several approximations, which omit certain potentially important contributions. For instance, the RPA polarization $\Pi_1(q)$ neglects the feedback effects of NFL behavior and Cooper pairing on nematic fluctuations. The electron self-energy $\Sigma_1(\epsilon_n)$ is only valid at low frequencies and at $T = 0$, and does not account for the feedback from the pairing gap.

Another common approximation is to consider only the electrons located exactly on Fermi surface^{58,62,68–70,73,74}, implemented by fixing the absolute value of the electron momentum \mathbf{p} at the Fermi momentum \mathbf{p}_F . Using this approximation, the pairing function is independent of momentum, which significantly reduces the difficulty of numerical computations. However, while this approximation is justified for the FL regime, it could result in considerable uncertainties in the gap size and T_c in the NFL regime, where the electrons occupy a sizeable portion of states off the Fermi surface. To determine the gap and T_c with higher precision, it is essential to maintain the contributions from the full range of electron momenta.

Furthermore, the nonlinear ME equations are often linearized near T_c based on the fact that the gap vanishes continuously as $T \rightarrow T_c$. Then the determination of T_c is converted into the calculation of the largest eigenvalue of a linear operator. It is clear that linearization is invalid at temperatures well below T_c . In Refs.^{66,69,70,74}, the nonlinear ME gap equations were solved directly, revealing new behaviors that cannot be derived from solutions of linearized equations. Nevertheless, these studies still adopted other approximations mentioned above.

The purpose of the present work is to examine how the previously obtained results on T_c are changed when the widely used approximations are removed. We will: (1) replace the simple RPA-level polarization $\Pi^{1L}(q)$ with the self-consistent $\Pi(q)$ determined from the DS equation of $D(q)$; (2) retain the mutual influence between Landau damping and Cooper pairing so as to treat NFL behavior

and superconductivity on an equal footing; (3) incorporate the contributions from the electrons resided not only on but also away from the Fermi surface; (4) include the contributions of vertex corrections in the determination of the superconducting T_c .

We now consider vertex corrections corresponding to triangle loop diagram. These vertex corrections have been inserted into the electron self-energy in studies on phonon-mediated superconductivity^{87,88}, while the free phonon propagator remaining unchanged. Here, in order to treat the electrons and the nematic fluctuations equally, we will incorporate vertex corrections into the DS equations of both $G(p)$ and $D(q)$. At the lowest (one-loop) order, the DS equation for the triangle vertex function $\Gamma_v^{1L}(p+q, p)$ has the expression

$$\begin{aligned} \Gamma_v^{1L}(p', p) = & g\sigma_3 + \frac{g^3}{f\left(\frac{\mathbf{p}+\mathbf{p}'}{2}\right)} \int_k f\left(\mathbf{p}' + \frac{\mathbf{k}}{2}\right) \\ & \times f\left(\frac{\mathbf{p} + \mathbf{p}'}{2} + \mathbf{k}\right) f\left(\mathbf{p} + \frac{\mathbf{k}}{2}\right) \\ & \times \sigma_3 D(k) G(p' + k) \sigma_3 G(p + k) \sigma_3. \end{aligned} \quad (14)$$

This $\Gamma_v^{1L}(p+q, p)$ enters into the DS equations of $G(p)$ and $D(q)$, which then become

$$\begin{aligned} G^{-1}(p) = & G_0^{-1}(p) + g \int_q f^2\left(\mathbf{p} + \frac{\mathbf{q}}{2}\right) D(q) \\ & \times \sigma_3 G(p+q) \Gamma_v^{1L}(p+q, p), \end{aligned} \quad (15)$$

$$\begin{aligned} D^{-1}(q) = & D_0^{-1}(q) - g \text{Tr} \int_p f^2\left(\mathbf{p} + \frac{\mathbf{q}}{2}\right) \\ & \times \sigma_3 G(p) \Gamma_v^{1L}(p+q, p) G(p+q),. \end{aligned} \quad (16)$$

A diagrammatic illustration of these DS equations is plotted in Fig. 1. Most of the uncertainties arising from the aforementioned approximations can be largely mitigated if the three integral equations of $\Gamma_v^{1L}(p+q, p)$, $G(p)$, and $D(q)$, given by Eqs. (14), (15), and (16), respectively, are numerically solved in a self-consistent manner.

The renormalized electron propagator $G(p)$ can be generically expressed as follows

$$G(p) = \frac{1}{A_1(\epsilon_n, \mathbf{p})\epsilon_n\sigma_0 - A_2(\epsilon_n, \mathbf{p})\xi_{\mathbf{p}}\sigma_3 + \Phi(\epsilon_n, \mathbf{p})\sigma_1}. \quad (17)$$

As demonstrated by Nambu⁷⁸, the σ_2 term needs not be considered. Quantum many-body effects and their interplay are encoded in the mass renormalization function $A_1(\epsilon_n, \mathbf{p})$, the chemical potential renormalization $A_2(\epsilon_n, \mathbf{p})$, and the pairing amplitude $\Phi(\epsilon_n, \mathbf{p})$. In particular, NFL behavior manifests itself in the frequency dependence of $A_1(\epsilon_n, \mathbf{p})$.

Substituting Eq. (17) into Eq. (14), Eq. (15), and Eq. (16), we decompose the equations of $G(p)$ into three self-consistent integral equations of $A_1(\epsilon_n, \mathbf{p})$, $A_2(\epsilon_n, \mathbf{p})$, and $\Phi(\epsilon_n, \mathbf{p})$ given by

$$A_1(\epsilon_n, \mathbf{p}) = 1 + \frac{T}{\epsilon_n} \sum_m \int \frac{d^2 \mathbf{q}}{(2\pi)^2} \tilde{\mathcal{K}}_v(\omega_m, \mathbf{q}, \epsilon_n, \mathbf{p}) A_1(\epsilon_n + \omega_m, \mathbf{p} + \mathbf{q})(\epsilon_n + \omega_m), \quad (18)$$

$$A_2(\epsilon_n, \mathbf{p}) = 1 - \frac{T}{\xi_{\mathbf{p}}} \sum_m \int \frac{d^2 \mathbf{q}}{(2\pi)^2} \tilde{\mathcal{K}}_v(\omega_m, \mathbf{q}, \epsilon_n, \mathbf{p}) A_2(\epsilon_n + \omega_m, \mathbf{p} + \mathbf{q}) \xi_{\mathbf{p}+\mathbf{q}}, \quad (19)$$

$$\Phi(\epsilon_n, \mathbf{p}) = T \sum_m \int \frac{d^2 \mathbf{q}}{(2\pi)^2} \tilde{\mathcal{K}}_v(\omega_m, \mathbf{q}, \epsilon_n, \mathbf{p}) \Phi(\epsilon_n + \omega_m, \mathbf{p} + \mathbf{q}). \quad (20)$$

Here, we have defined the following kernel function $\tilde{\mathcal{K}}_v$:

$$\begin{aligned} \tilde{\mathcal{K}}_v(\omega_m, \mathbf{q}, \epsilon_n, \mathbf{p}) &= \frac{g^2 f^2 \left(\mathbf{p} + \frac{\mathbf{q}}{2} \right)}{\omega_m^2/v_B^2 + |\mathbf{q}|^2 + r + \Pi(\omega_m, \mathbf{q})} \\ &\times \frac{\Gamma_v^{1L}(\epsilon_n + \omega_m, \mathbf{p} + \mathbf{q}, \epsilon_n, \mathbf{p})}{A_1^2(\epsilon_n + \omega_m, \mathbf{p} + \mathbf{q})(\epsilon_n + \omega_m)^2 + A_2^2(\epsilon_n + \omega_m, \mathbf{p} + \mathbf{q})\xi_{\mathbf{p}+\mathbf{q}}^2 + \Phi^2(\epsilon_n + \omega_m, \mathbf{p} + \mathbf{q})}. \end{aligned} \quad (21)$$

The polarization function $\Pi(\omega_m, \mathbf{q})$ that appears in Eq. (21) satisfies its own equation:

$$\begin{aligned} \Pi(\omega_m, \mathbf{q}) &= g^2 T \sum_n \int \frac{d^2 \mathbf{p}}{(2\pi)^2} \frac{f^2 \left(\mathbf{p} + \frac{\mathbf{q}}{2} \right) \Gamma_v^{1L}(\epsilon_n + \omega_m, \mathbf{p} + \mathbf{q}, \epsilon_n, \mathbf{p})}{A_1^2(\epsilon_n, \mathbf{p})\epsilon_n^2 + A_2^2(\epsilon_n, \mathbf{p})\xi_{\mathbf{p}}^2 + \Phi^2(\epsilon_n, \mathbf{p})} \\ &\times \frac{A_1(\epsilon_n + \omega_m, \mathbf{p} + \mathbf{q})(\epsilon_n + \omega_m)A_1(\epsilon_n, \mathbf{p})\epsilon_n - A_2(\epsilon_n + \omega_m, \mathbf{p} + \mathbf{q})\xi_{\mathbf{p}+\mathbf{q}}A_2(\epsilon_n, \mathbf{p})\xi_{\mathbf{p}} + \Phi(\epsilon_n + \omega_m, \mathbf{p} + \mathbf{q})\Phi(\epsilon_n, \mathbf{p})}{A_1^2(\epsilon_n + \omega_m, \mathbf{p} + \mathbf{q})(\epsilon_n + \omega_m)^2 + A_2^2(\epsilon_n + \omega_m, \mathbf{p} + \mathbf{q})\xi_{\mathbf{p}+\mathbf{q}}^2 + \Phi^2(\epsilon_n + \omega_m, \mathbf{p} + \mathbf{q})}. \end{aligned} \quad (22)$$

In principle, $\Pi(\omega_m, \mathbf{q})$ is expected to vanish in the zero-energy and zero-momentum limits, as required by conservation laws and the divergence of nematic propagator at the QCP where $r = 0$. However, generic theoretical analysis reveals that $\Pi(\omega_m = 0, \mathbf{q} \rightarrow 0)$ is not well defined, since its value depends on the order of integration^{3,72,89–97}. Specifically, $\Pi(\omega_m, \mathbf{q})$ may vanish or approach a certain constant Π_0 in the limits $\omega_m = 0$ and $\mathbf{q} \rightarrow 0$. Extensive studies have identified a constant Π_0 in various contexts, including $U(1)$ gauge theories^{89,90}, NFL behavior due to nematic critical fluctuations^{3,72,91–93}, charge- or spin-density wave quantum criticality^{94–96}, and interacting fermion system with a Bose surface⁹⁷. A common approach to addressing this problem is to subtract the constant Π_0 from $\Pi(\omega_m, \mathbf{q})$, which ensures that the effective polarization vanishes at $\omega_m = 0$ and $\mathbf{q} \rightarrow 0$. Here, we adopt this approach and redefine the polarization function as

$$\Pi(\omega_m, \mathbf{q}) - \Pi(\omega_m = 0, \mathbf{q} \rightarrow 0) \rightarrow \Pi(\omega_m, \mathbf{q}). \quad (23)$$

The vertex function $\Gamma_v^{1L}(\epsilon_{n'}, \mathbf{p}', \epsilon_n, \mathbf{p})$ fulfills its own integral equation:

$$\begin{aligned} \Gamma_v^{1L}(\epsilon_{n'}, \mathbf{p}', \epsilon_n, \mathbf{p}) &= g + g^3 T \sum_l \int \frac{d^2 \mathbf{k}}{2\pi^2} \frac{f^{-1} \left(\frac{\mathbf{p} + \mathbf{p}'}{2} \right) f(\mathbf{p}' + \frac{\mathbf{k}}{2}) f(\frac{\mathbf{p} + \mathbf{p}'}{2} + \mathbf{k}) f(\mathbf{p} + \frac{\mathbf{k}}{2})}{A_1^2(\epsilon_n + \omega_l, \mathbf{p} + \mathbf{k})\epsilon_l^2 + A_2^2(\epsilon_n + \omega_l, \mathbf{p} + \mathbf{k})\xi_{\mathbf{p}+\mathbf{k}}^2 + \Phi^2(\epsilon_n + \omega_l, \mathbf{p} + \mathbf{k})} \\ &\times \frac{[\omega_l^2/v_B^2 + |\mathbf{k}|^2 + r + \Pi(\omega_l, \mathbf{k})]^{-1}}{A_1^2(\epsilon_{n'} + \omega_l, \mathbf{p}' + \mathbf{k})(\epsilon_{n'} + \omega_l)^2 + A_2^2(\epsilon_{n'} + \omega_l, \mathbf{p}' + \mathbf{k})\xi_{\mathbf{p}'+\mathbf{k}}^2 + \Phi^2(\epsilon_{n'} + \omega_l, \mathbf{p}' + \mathbf{k})} \\ &\times \left[A_1(\epsilon_{n'} + \omega_l, \mathbf{p}' + \mathbf{k})(\epsilon_{n'} + \omega_l)A_1(\epsilon_n + \omega_l, \mathbf{p} + \mathbf{k})(\epsilon_n + \omega_l) - A_2(\epsilon_{n'} + \omega_l, \mathbf{p}' + \mathbf{k})\xi_{\mathbf{p}'+\mathbf{k}} \right. \\ &\left. \times A_2(\epsilon_n + \omega_l, \mathbf{p} + \mathbf{k})\xi_{\mathbf{p}+\mathbf{k}} + \Phi(\epsilon_{n'} + \omega_l, \mathbf{p}' + \mathbf{k})\Phi(\epsilon_n + \omega_l, \mathbf{p} + \mathbf{k}) \right]. \end{aligned} \quad (24)$$

The superconducting gap is defined as

$$\Delta(\epsilon_n, \mathbf{p}) = \frac{\Phi(\epsilon_n, \mathbf{p})}{A_1(\epsilon_n, \mathbf{p})}. \quad (25)$$

To facilitate numerical calculations, all the involved quantities are made dimensionless after performing the following re-scaling transformations:

$$A_1 \rightarrow A_1, \quad A_2 \rightarrow A_2, \quad T \rightarrow \frac{T}{E_F}, \quad \epsilon_n \rightarrow \frac{\epsilon_n}{E_F}, \quad \omega_m \rightarrow \frac{\omega_m}{E_F}, \quad (26)$$

$$\Phi \rightarrow \frac{\Phi}{E_F}, \quad g^2 \rightarrow \frac{g^2}{E_F}, \quad \mathbf{p} \rightarrow \frac{\mathbf{p}}{p_F}, \quad r \rightarrow \frac{r}{p_F^2}, \quad \xi_{\mathbf{p}} \rightarrow \frac{\xi_{\mathbf{p}}}{E_F} = \frac{\frac{\mathbf{p}^2 - p_F^2}{2m}}{\frac{p_F^2}{2m}} = \mathbf{p}^2 - 1. \quad (27)$$

III. NUMERICAL RESULTS

The effective model defined by Eq. 1 has been studied by Lederer *et al.*⁵⁸ and Chubukov *et al.*^{68–70} based on certain approximations, including the RPA polarization $\Pi_1(q)$ given by Eq. (12) and the Fermi-surface approximation. Lederer *et al.*⁵⁸ focused on the BCS-ME regime, characterized by a relatively large value of r , and found an obvious enhancement of superconductivity due to nematicity in both *s*-wave and *d*-wave channels. Klein and Chubukov⁶⁸ considered the deep NFL regime at the nematic QCP with $r = 0$. The renormalization factor $A_1(p)$ adopted in Ref.⁶⁸ was derived from the lowest self-energy $\Sigma_1(\epsilon_n)$ expressed in Eq. (13). In Refs.^{69,70}, the non-linear gap equation for $\Delta(\epsilon_n)$ was solved without using the linearization adopted in Ref.⁶⁸, although other conventional approximations were retained. Recently, the role of vertex corrections within an electron-nematic model has been examined by Zhang *et al.*⁷⁷ based on a simplified Ward identity. However, a systematic investigation of the influence of vertex corrections on the superconductivity driven by nematic fluctuations is still lacking.

Here, we re-visit the same model by going beyond some of previously used approximations. We will solve the non-linear integral equations given by Eqs. (18)-(24) using the iteration method demonstrated in Ref.⁹⁸. We will not introduce the Fermi-surface approximation, but instead allow the electron momentum $|\mathbf{p}|$ to span the full interval $[0, 2p_F]$. In all our calculations, the dimensionless coupling constant is fixed at $g = 0.45$.

To compute the integrals numerically, we discretize the three-dimensional space spanned by the Matsubara frequency ϵ_n , the absolute value of momentum $|\mathbf{p}|$, and the angle θ into small grid cells. These three variables are sampled at 42, 51, and 164 points, respectively. The task of solving self-consistent nonlinear integral equations are significantly beyond the capabilities of typical computer resources, primarily because the vertex function $\Gamma_v^{IL}(\epsilon_n', \mathbf{p}', \epsilon_n, \mathbf{p})$ has six variables. To reduce the computational burden in numerical integration, here we adopt a selective interpolation strategy to handle the large number of grid points. Among all the 42 frequency points, we retain only a reduced set of 12 points and approximate the other 30 points using the linear interpolation scheme, which effectively preserves the accuracy while greatly diminishing the computational cost. The same strategy can be applied to deal with $|\mathbf{p}|$ and θ . Among the 51 discrete points for $|\mathbf{p}|$ and 164 discrete points for θ , we retain 11 points for $|\mathbf{p}|$ and 36 points for θ . In particular, these points are retained adaptively, with a higher density allocated to the regions where the vertex function exhibits a pronounced variation. The computational burden can be further alleviated by exploiting the inherent symmetries of the vertex function. For instance, the integral can be evaluated only for a minimal set of representative directions, and the results can be mapped to all symmetry-equivalent directions via appropriate operations. Through all these optimizations, the

total computational time has been reduced by four to five orders of magnitude, bringing it down to an acceptable value.

To estimate the error induced by linear interpolation, we have computed T_c within ME theory for $g = 0.45$ and $r = 10^{-2}$. The interpolated and fully resolved values are $T_c = 0.0333$ and $T_c = 0.0335$, respectively. Therefore, linear interpolation leads to an error of $\approx 0.6\%$. For the same parameters $g = 0.45$ and $r = 10^{-2}$, the value of T_c obtained with vertex corrections is $T_c = 0.0285$, which is $\approx 15\%$ lower than the bare-vertex result $T_c = 0.0335$. Since the interpolation error is two orders of magnitude smaller than the vertex-correction effect, we adopt linear interpolation as a well-justified approximation.

While the self-consistent integral equations are equally applicable for any value of r , the numerical computations become increasingly more difficult as r decreases. For smaller values of r , it is necessary to choose more points for each integration variable. The computational time required to reach convergence is dramatically increased when r is lowered. To ensure the precision of the results, the value of r is restricted to the range of $r \geq 10^{-3}$.

After solving the integral equations (18)-(24), we have obtained the full frequency, momentum, and angular dependence of all four functions of $A_1(p)$, $A_2(p)$, $\Phi(p)$, and $\Pi(q)$. Their three-dimensional visualizations are rather cumbersome and do not convey clear information. Therefore, we will not show these color maps and instead focus on the symmetry of superconducting gap and the behavior of T_c , which are experimentally accessible and can be compared with existing data.

A. Superconducting gap symmetry

Although the form factor $\hat{f}(\theta)$ of the Yukawa coupling exhibits a *d*-wave angular dependence, the resulting pairing gap does not necessarily display *d*-wave symmetry⁵⁸. If the ME equations are linearized in the limit $T \rightarrow T_c$, which amounts to dropping Φ from the denominators, the value of T_c for each pairing channel is determined by the largest eigenvalue of the resultant linear equation. Klein and Chubukov⁶⁸ have found that *s*-wave and *d*-wave gaps are nearly degenerate at nematic QCP, but the T_c for *s*-wave symmetry is slightly higher than that for *d*-wave symmetry. Recently, a highly anisotropic *s*-wave superconducting gap has been observed⁹⁹ near the nematic QCP of $\text{FeSe}_{1-x}\text{S}_x$, which is qualitatively consistent with the gap symmetry predicted in Ref.⁶⁸.

To determine the pairing symmetry, here we solve the nonlinear integral equations by setting various initial values of $\Phi(p)$ and analyze the angular dependence of the convergent solutions for the superconducting gap $\Delta(p)$. One could assign a θ -independent constant initial value or an arbitrary θ -dependent function to $\Phi(p)$. Under the bare vertex approximation, our computations show that the nonlinear equations have only two possible solutions: an extended *s*-wave gap that is positive for all angles and

a sign-changing $d_{x^2-y^2}$ -wave gap. A $d_{x^2-y^2}$ -wave solution is obtained if and only if a pure $d_{x^2-y^2}$ -wave initial value of $\Phi(p)$ is assumed. However, this pure $d_{x^2-y^2}$ -wave solution is fragile. When the initial value of $\Phi(p)$ is different from a pure $d_{x^2-y^2}$ -wave form, the solution of $\Phi(p)$ inevitably evolves into an extended s -wave gap. Moreover, once vertex corrections are incorporated, the extended s -wave pairing emerges as the sole stable solution for all possible initial values of $\Phi(p)$.

In Fig. 2, we depict the detailed θ -dependence of $A_1(\theta)$,

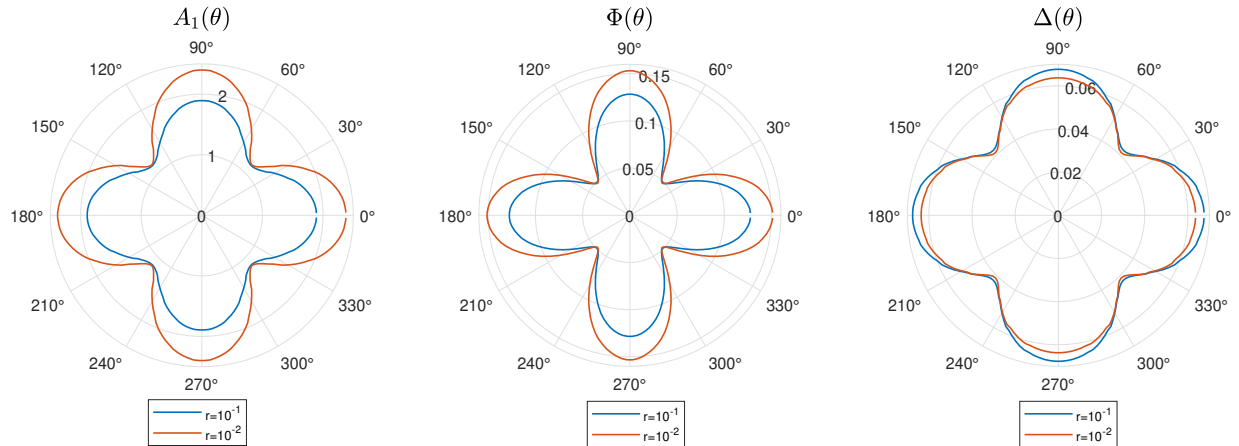


FIG. 2: Angular dependence of $A_1(\theta)$, $\Phi(\theta)$, and $\Delta(\theta)$ at the frequency $\epsilon_n = \pi T$ and the Fermi momentum \mathbf{p}_F . Other model parameters are $g = 0.45$ and $T = 0.01$. Blue and orange-red curves correspond to $r = 10^{-1}$ and $r = 10^{-2}$, respectively.

Recent muon spin relaxation measurements⁴⁰ have provided experimental evidence that, for $x \leq 0.22$, the $\text{FeSe}_{1-x}\text{S}_x$ superconductor hosts a superconducting state in which time-reversal symmetry is spontaneously broken. Our numerical computations yield no indication of such an unconventional pairing state. Probably, the simple single-band model under consideration lacks certain degrees of freedom or interactions that are essential for realizing time-reversal-symmetry breaking.

B. Dependence of T_c on r

To clarify how the critical temperature T_c is influenced by various theoretical ingredients, we compare the results obtained under three different approximations.

- VERTEX: T_c is determined by solving the fully self-consistent DS equations given by (18)-(24) without any additional approximations.

- ME: The DS equations are simplified to the ME equations for $G(p)$ and $D(q)$ after adopting the bare vertex approximation, i.e. replacing the vertex function $\Gamma_v^{1L}(\epsilon_{n'}, \mathbf{p}', \epsilon_n, \mathbf{p})$ with $g_0 \sigma_3$.

$\Phi(\theta)$, and $\Delta(\theta)$ at the frequency $\epsilon_n = \pi T$ and at the Fermi momentum. The s -wave gap obtained in our calculations aligns with the results of Klein and Chubukov⁶⁸ and is also consistent with the observation reported by Nag *et al.*⁹⁹. The gap observed by Nag *et al.*⁹⁹ is highly anisotropic and nearly nodal. In comparison, the gap shown in Fig. 2 exhibits merely a moderate anisotropy, probably because the values of r used in our calculations are not sufficient small.

- MEFS: The ME equations are further simplified by fixing the electron momentum at the Fermi momentum (i.e., Fermi-surface approximation).

The resulting T_c for each case is shown in Fig. 3. It can be seen that neglecting vertex corrections tends to overestimate T_c . The introduction of Fermi surface approximation leads to a more significant overestimation of T_c . An apparent indication is that the contributions of the electrons off the Fermi surface make important contributions to the formation of superconductivity.

Under the bare vertex approximation, for either ME or MEFS curve, the corresponding T_c is a monotonously decreasing function of r . This implies that superconductivity is always enhanced as the system gets closer to the nematic QCP. However, the behavior of $T_c(r)$ is qualitatively changed when the vertex corrections are taken into account. According to the VERTEX curve shown in Fig. 3, as r decreases from 10^{-1} to 10^{-3} , T_c first increases but then decreases after passing through its maximal value. Therefore, the function $T_c(r)$ determined in the presence of vertex corrections exhibits a non-monotonic dependence on the distance to the nematic QCP.

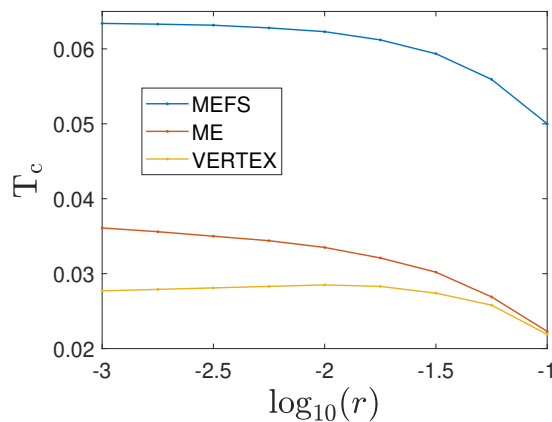


FIG. 3: Superconducting transition temperature T_c as a function of the parameter r for $g = 0.45$. The blue, orange-red, and yellow curves correspond to the MEFS, ME, and VERTEX approximations, respectively. $T_c = 0$ if r becomes sufficiently large.

Since the value of T_c is only moderately suppressed as r is decreased in the range $r < 10^{-2}$, it is necessary to examine whether the non-monotonic behavior of $T_c(r)$ is changed if other interpolation methods are adopted. We employ three distinct linear interpolation methods, labeled as LIN-I, LIN-II, and LIN-III, to compute T_c , and list the original results in Table I. The total numbers of sampling points for $(\epsilon_n, |\mathbf{p}|, \theta)$ are fixed at $(42, 51, 164)$ for each method. However, the number of selected sparse sampling points are different. The corresponding $T_c(r)$ curves are presented in Fig. 4. Although different interpolation schemes result in slight variations in the values of T_c , the non-monotonic behavior of $T_c(r)$ is observed for all interpolation schemes. Furthermore, we have also gone beyond the linear interpolation and employed a more accurate local quadratic interpolation (LQI)¹⁰⁰. The computational time required for LQI is roughly ten times longer than that for linear interpolation methods. Since our goal is to verify the reliability of the non-monotonicity of $T_c(r)$, we have chosen only two representative values of r in LQI calculations: $r = 10^{-2}$ and $r = 10^{-3}$. The results presented in Table I and Fig. 4 demonstrate that the non-monotonicity of $T_c(r)$ is a robust feature rather than an artifact of the linear interpolation approximation.

Owing to computational limitations, we have not achieved converged solutions of the nonlinear integral equations for $r < 10^{-3}$. The behavior of $T_c(r)$ in this regime remains unknown. To get reliable results of T_c in this region, the space spanned by ϵ_n , $|\mathbf{p}|$, and θ should be discretized into smaller grids, which will substantially increase the computational time.

It is important to find out the origin of the striking non-monotonic evolution of $T_c(r)$. We fix the electron momenta on the Fermi surface, i.e., $\mathbf{p} = \mathbf{p}_F$, and compare the r -dependence of $A_1(\epsilon_n)$ with that of $\Phi(\epsilon_n)$. From the

results shown in Fig. 5 (a)-(b), we find that the reduction of r gives rise to a monotonic increase in both $A_1(\epsilon_n)$ and $\Phi(\epsilon_n)$. Thus, the NFL behavior and Cooper pairing are both enhanced as the nematic QCP is approached. Nevertheless, it is important to notice that the superconducting gap $\Delta(\epsilon_n)$ is the ratio $\Phi(\epsilon_n)/A_1(\epsilon_n)$ rather than $\Phi(\epsilon_n)$. The gap size can be suppressed when $A_1(\epsilon_n)$ is enhanced more significantly than $\Phi(\epsilon_n)$. To display the r -dependence of gap size, we also plot the function of $\Delta(\epsilon_n)$ for $r = 10^{-1}$, $r = 10^{-2}$, and $r = 10^{-3}$ in Fig. 5(c). One can see that the superconducting gap determined at $r = 10^{-2}$ is larger than those determined at $r = 10^{-1}$ and $r = 10^{-3}$. The non-monotonic r -dependence of the gap size eventually results in the non-monotonic r -dependence of T_c . These results suggest the presence of an intricate interplay between NFL behavior and Cooper pairing near nematic QCP.

TABLE I: Results of T_c determined using four different interpolation methods. The numbers given in the columns of ϵ_n , $|\mathbf{p}|$, and θ represent the numbers of the selected sparse sampling points. The error in the LQI results for $r = 0.001$ becomes larger because the required computational effort increases substantially.

Method	T_c	Error	ϵ_n	$ \mathbf{p} $	θ	r
LIN-I	0.0219	± 0.0001	12	11	36	10^{-1}
LIN-II	0.0221	± 0.0001	12	11	20	10^{-1}
LIN-III	0.0223	± 0.0001	10	11	36	10^{-1}
LIN-I	0.0283	± 0.0001	12	11	36	2×10^{-2}
LIN-II	0.0285	± 0.0001	12	11	20	2×10^{-2}
LIN-III	0.0284	± 0.0001	10	11	36	2×10^{-2}
LIN-I	0.0285	± 0.0001	12	11	36	10^{-2}
LIN-II	0.0287	± 0.0001	12	11	20	10^{-2}
LIN-III	0.0289	± 0.0001	10	11	36	10^{-2}
LIN-I	0.0277	± 0.0001	12	11	36	10^{-3}
LIN-II	0.0281	± 0.0001	12	11	20	10^{-3}
LIN-III	0.0283	± 0.0001	10	11	36	10^{-3}
LQI	0.0289	± 0.0001	12	11	36	10^{-2}
LQI	0.0278	± 0.0004	12	11	36	10^{-3}

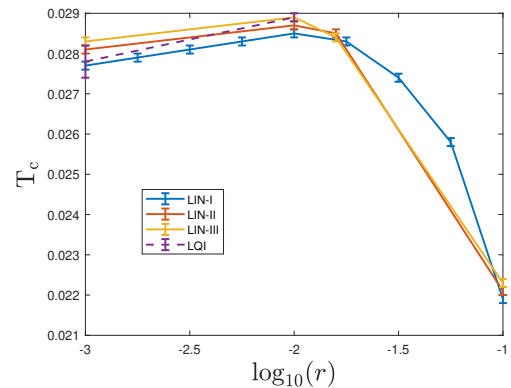


FIG. 4: Curves of $T_c(r)$ with error bars. Here, $g = 0.45$.

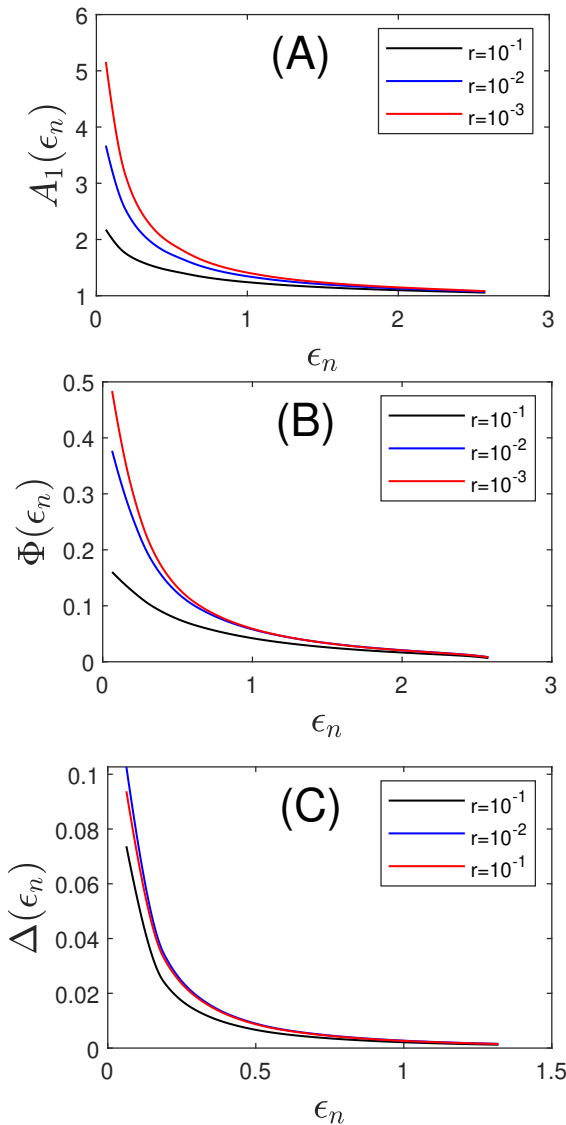


FIG. 5: The frequency dependence of $A_1(\epsilon_n)$, $\Phi(\epsilon_n)$, and $\Delta(\epsilon_n) = \Phi(\epsilon_n)/A_1(\epsilon_n)$ in the $\theta = 0$ direction for electrons restricted on the Fermi surface. The results are obtained for $g = 0.45$ and $T = 0.02$.

C. Comparison with experiments

Early theoretical works^{56–59} predicted a pronounced enhancement of the superconducting T_c at the nematic QCP, where the pairing interaction mediated by nematic fluctuations is strongest. This prediction has been extensively tested in iron-based superconductors. In the BaFeAs family, the nematic order usually coexists with antiferromagnetic spin-density-wave (SDW) order, and the resulting entanglement of the nematic and magnetic fluctuations obscures their individual effects on superconductivity. It appears more suitable to explore the relationship between nematicity and superconductivity in FeSe superconductors due to the absence of SDW order

at ambient pressure.

Over the past decade, there has been a surge of experimental studies^{18,19,28–43} on the properties of superconductivity emerging around the nematic QCP in $\text{FeSe}_{1-x}\text{S}_x$ and $\text{FeSe}_{1-x}\text{Te}_x$ systems. Contrary to theoretical expectations, the value of T_c is typically not obviously boosted at the nematic QCP, irrespective of whether nematic order is destroyed by chemical substitution or the variation of pressure.

Some recent works have attributed the absence of significant enhancement of T_c at nematic QCP to the effects of nematoelastic coupling^{35,37,101–104}. Labat and Paul¹⁰² defined a dimensionless parameter r_0 to represent the effective strength of nematoelastic coupling and then demonstrated that T_c is strongly enhanced only when the condition $r_0 \ll (U/V)^2$ is fulfilled, where U measures the pairing interaction strength generated by nematic fluctuations and V collects all the non-nematic contributions (such as magnetic fluctuations or phonons). When this inequality is reversed, namely $r_0 \gg (U/V)^2$, the increase of T_c is modest even at the QCP. Applying this criterion to $\text{FeSe}_{1-x}\text{S}_x$, where strong magnetic fluctuations yield a sizeable V , the absence of appreciable T_c enhancement at the nematic QCP $x = 0.17$ can be naturally explained^{35,37}. The situation is distinct in $\text{FeSe}_{1-x}\text{Te}_x$, which displays a clear superconducting dome^{36,37,39} in the vicinity of nematic QCP defined at $x_c = 0.50$ at ambient pressure. Since no magnetic fluctuations were detected within the same doping region^{36,37}, implying that $V = 0$, it is likely that the superconducting dome is solely induced by nematic fluctuations. According to Labat-Paul criterion^{37,102}, T_c should be strongly enhanced at the QCP, regardless of whether the nematoelastic coupling is weak or strong.

However, the superconducting dome observed in $\text{FeSe}_{1-x}\text{Te}_x$ exhibits an anomalous shape^{36,37,39}: T_c is not maximal at the nematic QCP ($x_c = 0.50$), but peaks at a higher Te concentration $x_p \approx 0.60$. This displacement of the optimal doping ($x_p \approx 0.60$) away from the nematic QCP, together with the unusual suppression of T_c at the QCP, is incompatible with the theories predicting the maximum T_c to occur precisely at the QCP^{56–59}. Furthermore, this observation cannot be reconciled with the scenario of nematoelastic coupling¹⁰², which allows only for an increase in T_c at the QCP. In Ref.³⁶, the authors speculated that such a difference may originate from the more significant enhancement of quasiparticle damping effects than the pairing interaction.

According to our results, the transition temperature T_c determined after including vertex corrections displays a non-monotonic r -dependence: T_c is peaked at a finite r_m rather than at the nematic QCP ($r = 0$). In the region of $0 < r < r_m$, T_c is gradually suppressed as r is lowered. This behavior provides a possible interpretation of the salient features T_c observed on the disordered side of the nematic QCP in $\text{FeSe}_{1-x}\text{Te}_x$, including the discrepancy between the optimal doping and the nematic QCP and the anomalous suppression of T_c as the system is

approaching to QCP.

As illustrated in Fig. 5, the decrease of r enhances both the NFL behavior, embodied in $A_1(\epsilon_n)$, and the pairing strength, measured by $\Phi(\epsilon_n)$, but the NFL behavior is enhanced more significantly as $r \rightarrow 0$. It turns out that the non-monotonic $T_c(r)$ curve is generated by the subtle interplay of NFL decoherence and Cooper pairing of strongly damped electrons. This lends a quantitative support to the scenario proposed in Ref.³⁶ and highlights the pivotal role of vertex corrections in capturing the interplay of different quantum many-body effects.

Our present analysis is applicable solely to the disordered (tetragonal) side of nematic QCP. The ordered (orthorhombic) side may exhibit qualitatively different properties. For instance, the Fermi surface distortion caused by nematic order could lead to effects absent in the disordered side. Moreover, there are experimental evidences^{32,33} suggesting that the superconducting gap in $\text{FeSe}_{1-x}\text{S}_x$ has distinct structures on the disordered and ordered sides of nematic QCP. In $\text{FeSe}_{1-x}\text{Te}_x$, the superconducting dome emerging in the doping region $x > 0.30$ also displays different features from the smaller superconducting dome observed deep inside the nematic phase³⁷. The physical origin of such distinctions remains elusive and awaits further research. The possible competition between nematicity and superconductivity¹⁰⁵ further complicates the situation.

IV. SUMMARY AND DISCUSSION

In summary, we studied the properties of the superconductivity formed in the vicinity of a two-dimensional Ising-type nematic QCP. Focusing on the disordered side of the transition, we treat the NFL behavior and Cooper pairing on an equal footing by solving the self-consistent nonlinear DS equations for the electron and nematic propagators and the lowest-order vertex correction without adopting further approximations. The only stable solution is an extended s -wave gap. Our calculations showed that vertex corrections qualitatively alter how the superconducting T_c evolves as the system is tuned to approach the nematic QCP from the disordered side. Under the bare-vertex approximation, T_c is always enhanced. After including vertex corrections, T_c exhibits a non-monotonic dependence on the distance to nematic QCP and its maximum is displaced from the QCP. This result provides a possible explanation for the anomalous evolution of T_c observed in the tetragonal phase of $\text{FeSe}_{1-x}\text{Te}_x$. We demonstrated that the non-monotonic evolution of T_c stems from a delicate interplay between NFL decoherence and Cooper pairing. Such an interplay

is hidden under the bare-vertex approximation and can be unveiled only when the vertex corrections are taken into account, suggesting the necessity of incorporating vertex corrections into the ME theory.

The analysis presented in this paper can be improved along the following directions:

(i) Our vertex corrections to the Yukawa coupling are presently limited to the lowest-order triangle diagrams. While even this minimal inclusion already reveals qualitatively new features in T_c , a systematic treatment of higher-order contributions is required. It is especially important to develop efficient schemes that can incorporate vertex corrections while preserving the Ward-Takahashi identities.

(ii) Nematic quantum criticality is currently treated based on a single-band model. This simplification is ideal for examining how vertex corrections modify the ME theory. However, it cannot capture the complicated multi-orbital electronic structures found in realistic materials, such as $\text{FeSe}_{1-x}\text{S}_x$ and $\text{FeSe}_{1-x}\text{Te}_x$. To provide a faithful account of these superconductors, the single-band model should be extended to incorporate the multi-orbital degrees of freedom^{106,107} and the competition and coexistence of nematic and superconducting orders¹⁰⁵. It would be of interest to study whether including the multi-orbital effects can lead to time-reversal symmetry broken superconducting states.

(iii) Solving the nonlinear integral equations with higher precision demands a more efficient algorithm. Very close to the nematic QCP ($r < 10^{-3}$), both NFL behavior and Cooper pairing are governed by small- $|\mathbf{q}|$ scattering, which requires a much finer grid in the $(\epsilon_n, |\mathbf{p}|, \theta)$ space. However, as the mesh is refined, the computational time required to reach convergent results of T_c is substantially increased. Furthermore, the nonlinear equations would become even more complicated after considering the multi-orbital effects. Balancing the accuracy and the computational cost calls for a further algorithmic optimization.

V. ACKNOWLEDGEMENT

We thank Hao-Fu Zhu for helpful discussions. This work is supported by the Anhui Natural Science Foundation under Grant 2208085MA11. J.R.W. acknowledges the support by the National Natural Science Foundation of China under Grant 12274414. The numerical calculations in this paper have been done on the supercomputing system in the Supercomputing Center of University of Science and Technology of China.

* Corresponding author: gzliu@ustc.edu.cn

¹ S. A. Kivelson, E. Fradkin, and V. Emery, Electronic

liquid-crystal phases of a doped Mott insulator, *Nature* (London) **393**, 550 (1998).

² V. Oganesyan, S. A. Kivelson, and E. Fradkin, Quantum theory of a nematic Fermi fluid, *Phys. Rev. B* **64**, 195109 (2001).

³ W. Metzner, D. Rohe, and S. Andergassen, Soft Fermi Surfaces and Breakdown of Fermi-Liquid Behavior, *Phys. Rev. Lett.* **91**, 066402 (2003).

⁴ Y. Ando, K. Segawa, S. Komiya, and A. N. Lavrov, Electrical resistivity anisotropy from self-Organized one dimensionality in high-temperature superconductors, *Phys. Rev. Lett.* **88**, 137005 (2002).

⁵ E. Fradkin, S. A. Kivelson, and J. M. Tranquada, Colloquium: Theory of intertwined orders in high temperature superconductors, *Rev. Mod. Phys.* **87**, 457 (2015).

⁶ B. Keimer, S. A. Kivelson, M. R. Norman, S. Uchida, and J. Zaanen, From quantum matter to high-temperature superconductivity in copper oxides, *Nature (London)* **518**, 179 (2015).

⁷ V. Hinkov, D. Haug, B. Fauqué, P. Bourges, Y. Sidis, A. Ivanov, C. Bernhard, C. T. Lin, and B. Keimer, Electronic liquid crystal state in the high-temperature superconductor $\text{YBa}_2\text{Cu}_3\text{O}_{6.45}$, *Science* **319**, 597 (2008).

⁸ R. Daou, J. Chang, D. LeBoeuf, O. Cyr-Choinière, F. Laliberté, N. Doiron-Leyraud, B. J. Ramshaw, R. Liang, D. A. Bonn, W. N. Hardy, and L. Taillefer, Broken rotational symmetry in the pseudogap phase of a high- T_c superconductor, *Nature (London)* **463**, 519 (2010).

⁹ M. J. Lawler, K. Fujita, J. Lee, A. R. Schmidt, Y. Kohsaka, C. K. Kim, H. Eisaki, S. Uchida, J. C. Davis, J. P. Sethna, and E. A. Kim, Intra-unit-cell electronic nematicity of the high- T_c copper-oxide pseudogap states, *Nature (London)* **466**, 347 (2010).

¹⁰ Y. Sato, S. Kasahara, H. Murayama, Y. Kasahara, E.-G. Moon, T. Nishizaki, T. Loew, J. Porras, B. Keimer, T. Shibauchi, and T. Matsuda, Thermodynamic evidence for a nematic phase transition at the onset of the pseudogap in $\text{YBa}_2\text{Cu}_3\text{O}_y$, *Nat. Phys.* **13**, 1074 (2017).

¹¹ J. Wu, A. T. Bollinger, X. He, and I. Božović, Spontaneous breaking of rotational symmetry in copper oxide superconductors, *Nature (London)* **547**, 432 (2017).

¹² N. Auvray, S. Benhabib, M. Cazayous, R. D. Zhong, J. Schneeloch, G. D. Gu, A. Forget, D. Colson, I. Paul, A. Sacuto, and Y. Gallais, Nematic fluctuations in the cuprate superconductor $\text{Bi}_2\text{Sr}_2\text{CaCu}_2\text{O}_{8+\delta}$, *Nat. Commun.* **10**, 5209 (2019).

¹³ S. Mukhopadhyay, R. Sharma, C. K. Kim, S. D. Edkins, M. H. Hamidian, H. Eisaki, Shin-ichi Uchida, E.-A. Kim, M. J. Lawler, A. P. Mackenzie, J. C. Séamus Davis, and K. Fujita, Evidence for a vestigial nematic state in the cuprate pseudogap phase, *Proc. Natl. Acad. Sci.* **116**, 13249 (2019).

¹⁴ K. Ishida, S. Hosoi, Y. Teramoto, T. Usui, Y. Mizukami, K. Itaka, Y. Matsuda, T. Watanabe, and T. Shibauchi, Divergent nematic susceptibility near the pseudogap critical point in a cuprate superconductor, *J. Phys. Soc. Jpn.* **89**, 064707 (2020).

¹⁵ A. Chubukov, Pairing mechanism in Fe-based superconductors, *Ann. Rev. Condens. Matter Phys.* **3**, 57 (2012).

¹⁶ R. M. Fernandes, A. V. Chubukov, and J. Schmalian, Nematic order in iron superconductors: who is in the driver seat? *Nat. Phys.* **10**, 97 (2014).

¹⁷ T. Shibauchi, A. Carrington, and Y. Matsuda, A quantum critical point lying beneath the superconducting dome in iron pnictides, *Ann. Rev. Condens. Matter Phys.* **5**, 113 (2014).

¹⁸ A. Coldea and M. D. Watson, The key ingredients of the electronic structure of FeSe, *Ann. Rev. Condens. Matter Phys.* **9**, 125 (2018).

¹⁹ A. E. Böhmer and A. Kreisel, Nematicity, magnetism and superconductivity in FeSe, *J. Phys. Condens. Matter* **30**, 023001 (2017).

²⁰ T.-M. Chuang, M. P. Allan, J. Lee, Y. Xie, N. Ni, S. L. Bud'ko, G. S. Boebinger, P. C. Canfield, J. C. Davis, Nematic electronic structure in the parent state of the Iron-based superconductor $\text{Ca}(\text{Fe}_{1-x}\text{Co}_x)_2\text{As}_2$, *Science* **327**, 181 (2010).

²¹ J.-H. Chu, J. G. Analytis, K. De Greve, P. L. McMahon, Z. Islam, Y. Yamamoto, and I. R. Fisher, In-plane resistivity anisotropy in an underdoped iron Arsenide superconductor, *Science* **329**, 824 (2010).

²² C.-L. Song, Y.-L. Wang, P. Cheng, Y.-P. Jiang, W. Li, T. Zhang, Z. Li, K. He, L. Wang, J.-F. Jia, H.-H. Hung, C. Wu, X. Ma, X. Chen, and Q.-K. Xue, Direct observation of nodes and twofold symmetry in FeSe superconductor, *Science* **332**, 1410 (2011).

²³ S. Kasahara, H. J. Shi, K. Hashimoto, S. Tonegawa, Y. Mizukami, T. Shibauchi, K. Sugimoto, T. Fukuda, T. Terashima, A. H. Nevidomsky, and Y. Matsuda, Electronic nematicity above the structural and superconducting transition in $\text{BaFe}_2(\text{As}_{1-x}\text{P}_x)_2$, *Nature (London)* **486**, 328 (2012).

²⁴ X. Lu, J. T. Park, R. Zhang, H. Luo, A. H. Nevidomsky, Q. Si, and P. Dai, Nematic spin correlations in the tetragonal state of uniaxial-strained $\text{BaFe}_{2-x}\text{Ni}_x\text{As}_2$, *Science* **345**, 657 (2014).

²⁵ S.-H. Baek, D. V. Efremov, J. M. Ok, J. S. Kim, J. van den Brink, and B. Büchner, Orbital-driven nematicity in FeSe, *Nat. Mat.* **14**, 210 (2015).

²⁶ H.-H. Kuo, J.-H. Chu, J. C. Palmstrom, S. A. Kivelson, and I. R. Fisher, Ubiquitous signatures of nematic quantum criticality in optimally doped Fe-based superconductors, *Science* **352**, 358 (2016).

²⁷ T. Worasaran, M. S. Ikeda, J. C. Palmstrom, J. A. W. Straquadine, S. A. Kivelson, I. R. Fisher, Nematic quantum criticality in an Fe-based superconductor revealed by strain-tuning, *Science* **372**, 793 (2021).

²⁸ S. Hosoi, K. Matsuura, K. Ishida, H. Wang, Y. Mizukami, T. Watashige, S. Kasahara, Y. Matsuda, and T. Shibauchi, Nematic quantum critical point without magnetism in $\text{FeSe}_{1-x}\text{S}_x$ superconductors, *Proc. Natl. Acad. Sci. (USA)* **113**, 8139 (2016).

²⁹ J. P. Sun, K. Matsuura, G. Z. Ye, Y. Mizukami, M. Shimozawa, K. Matsubayashi, M. Yamashita, T. Watashige, S. Kasahara, Y. Matsuda, J.-Q. Yan, B. C. Sales, Y. Uwatoko, J.-G. Cheng, and T. Shibauchi, Dome-shaped magnetic order competing with high-temperature superconductivity at high pressures in FeSe, *Nat. Communications* **7**, 12146 (2016).

³⁰ K. Matsuura, Y. Mizukami, Y. Arai, Y. Sugimura, N. Maejima, A. Machida, T. Watanuki, T. Fukuda, T. Yamada, Z. Hiroi, K. Y. Yip, Y. C. Chan, Q. Niu, S. Hosoi, K. Ishida, K. Mukasa, S. Kasahara, J.-G. Cheng, S. K. Goh, Y. Matsuda, Y. Uwatoko, and T. Shibauchi, Maximizing T_c by tuning nematicity and magnetism in $\text{FeSe}_{1-x}\text{S}_x$ superconductors, *Nat. Communications* **8**, 1143 (2017).

³¹ P. Wiecki, K. Rana, A. E. Böhmer, Y. Lee, S. L. Bud'ko, P. C. Canfield, and Y. Furukawa, Persistent correlation between superconductivity and antiferromagnetic fluctuations near a nematic quantum critical point in $\text{FeSe}_{1-x}\text{S}_x$,

Phys. Rev. B **98**, 020507(R) (2018).

³² Y. Sato, S. Kasahara, T. Taniguchi, X. Xing, Y. Kasahara, Y. Tokiwa, Y. Yamakawa, H. Kontani, T. Shibauchi, and Y. Matsuda, Abrupt change of the superconducting gap structure at the nematic critical point in $\text{FeSe}_{1-x}\text{S}_x$, Proc. Natl. Acad. Sci. (USA) **115**, 1227 (2018).

³³ T. Hanaguri, K. Iwaya, Y. Kohsaka, T. Machida, T. Watashige, S. Kasahara, T. Shibauchi, Y. Matsuda, Two distinct superconducting pairing states divided by the nematic end point in $\text{FeSe}_{1-x}\text{S}_x$, Sci. Adv. **4**, eaar6419 (2018).

³⁴ P. Reiss, D. Graf, A. A. Haghishirad, W. Knafo, L. Drigo, M. Bristow, A. J. Schofield, and A. I. Coldea, Quenched nematic criticality and two superconducting domes in an iron-based superconductor, Nat. Phys. **16**, 89 (2020).

³⁵ S. Chibani, D. Farina, P. Massat, M. Cazayous, A. Sacuto, T. Urata, Y. Tanabe, K. Tanigaki, A. E. Böhmer, P. C. Canfield, M. Merz, S. Karlsson, P. Strobel, P. Toulemonde, I. Paul, and Y. Gallais, Lattice-shifted nematic quantum critical point in $\text{FeSe}_{1-x}\text{S}_x$, npj Quantum Materials **6**, 37 (2021).

³⁶ K. Mukasa, K. Matsuura, M. Qiu, M. Saito, Y. Sugimura, K. Ishida, M. Otani, Y. Onishi, Y. Mizukami, K. Hashimoto, J. Gouchi, R. Kumai, Y. Uwatoko, and T. Shibauchi, High-pressure phase diagrams of $\text{FeSe}_{1-x}\text{Te}_x$: correlation between suppressed nematicity and enhanced superconductivity, Nat. Commun. **12**, 381 (2021).

³⁷ K. Ishida, Y. Onishi, M. Tsujii, K. Mukasa, M. Qiu, M. Saito, Y. Sugimura, K. Matsuura, Y. Mizukami, K. Hashimoto, and T. Shibauchi, Pure nematic quantum critical point accompanied by a superconducting dome, Proc. Natl. Acad. Sci. (USA) **119**, e2110501119 (2022).

³⁸ C. A. Occhialini, J. J. Sanchez, Q. Song, G. Fabbris, Y. Choi, J.-W. Kim, P. J. Ryan, and R. Comin, Spontaneous orbital polarization in the nematic phase of FeSe , Nat. Mat. **22**, 985 (2023).

³⁹ K. Mukasa, K. Ishida, S. Imajo, M. Qiu, M. Saito, K. Matsuura, Y. Sugimura, S. Liu, Y. Uezono, T. Otsuka, M. Čulo, S. Kasahara, Y. Matsuda, N. E. Hussey, T. Watanabe, K. Kindo, and T. Shibauchi, Enhanced superconducting pairing strength near a pure nematic quantum critical point, Phys. Rev. X **13**, 011032 (2023).

⁴⁰ K. Matsuura, M. Roppongi, M. Qiu, Q. Sheng, Y. Cai, K. Yamakawa, Z. Guguchia, R. P. Day, K. M. Kojima, A. Damascelli, Y. Sugimura, M. Saito, T. Takenaka, K. Ishihara, Y. Mizukami, K. Hashimoto, Y. Gu, S. Guo, L. Fu, Z. Zhang, F. Ning, G. Zhao, G. Dai, C. Jin, J. W. Beare, G. M. Luke, Y. J. Uemura, and T. Shibauchi, Two superconducting states with broken time-reversal symmetry in $\text{FeSe}_{1-x}\text{S}_x$, Proc. Natl. Acad. Sci. (USA) **120**, e2208276120 (2023).

⁴¹ P. Reiss, A. McCollam, Z. Zajicek, A. A. Haghishirad, and A. I. Coldea, Collapse of metallicity and high- T_c superconductivity in the high-pressure phase of $\text{FeSe}_{0.89}\text{S}_{0.11}$, npj Quantum Materials **9**, 73 (2024).

⁴² Q.-P. Ding, J. Schmidt, J. A. Moreno, S. L. Bud'ko, P. C. Canfield, and Yuji Furukawa, Role of nematic fluctuations on superconductivity in $\text{FeSe}_{0.47}\text{Te}_{0.53}$ revealed by nuclear magnetic resonance under pressure, Phys. Rev. Lett. **134**, 226002 (2025).

⁴³ M. Roppongi, Y. Cai, K. Ogawa, S. Liu, G. Q. Zhao, M. Oudah, T. Fujii, K. Imamura, S. Fang, K. Ishihara, K. Hashimoto, K. Matsuura, Y. Mizukami, M. Pula, C. Young, I. Markovic, D. A. Bonn, T. Watanabe, A. Yamashita, Y. Mizuguchi, G. M. Luke, K. M. Kojima, Y. J. Uemura, and T. Shibauchi, Topology meets time-reversal symmetry breaking in $\text{FeSe}_{1-x}\text{S}_x$ superconductor, arXiv:2501.02818.

⁴⁴ F. Ronning, T. Helm, K. R. Shirer, M. D. Bachmann, L. Balicas, M. K. Chan, B. J. Ramshaw, R. D. McDonald, F. F. Balakirev, M. Jaime, E. D. Bauer, and P. J. W. Moll, Electronic in-plane symmetry breaking at field-tuned quantum criticality in CeRhIn_5 , Nature (London) **548**, 313 (2017).

⁴⁵ J. Wu, H. P. Nair, A. T. Bollinger, X. He, I. Robinson, N. J. Schreiber, K. M. Shen, D. G. Schlom, and I. Božović, Electronic nematicity in Sr_2RuO_4 , Proc. Natl. Acad. Sci. (USA), **117**, 10654 (2020).

⁴⁶ L. Nie, S. Sun, W. Ma, D. Song, L. Zhang, Z. Liang, P. Wu, F. Yu, J. Li, M. Shan, D. Zhao, S. Li, B. Kang, Z. Wu, Y. Zhou, K. Liu, Z. Xiang, Z. Yang, Z. Wang, T. Wu, and X. Chen, Charge-density-wave-driven electronic nematicity in a kagome superconductor, Nature (London) **604**, 59 (2022).

⁴⁷ P. Wu, Y. Tu, Z. Wang, S. Yu, H. Li, W. Ma, Z. Liang, Y. Zhang, X. Zhang, Z. Li, Y. Yang, Z. Qiao, J. Ying, T. Wu, L. Shan, Z. Xiang, Z. Wang, and X. Chen, Unidirectional electron-phonon coupling in the nematic state of a kagome superconductor, Nat. Phys. **19**, 1143 (2023).

⁴⁸ Y. Hu, C. Le, Y. Zhang, Z. Zhao, J. Liu, J. Ma, N. C. Plumb, M. Radovic, H. Chen, A. P. Schnyder, X. Wu, X. Dong, J. Hu, H. Yang, H.-J. Gao, M. Shi, Non-trivial band topology and orbital-selective electronic nematicity in a titanium-based kagome superconductor, Nat. Phys. **19**, 1827 (2023).

⁴⁹ Y. Cao, D. Rodan-Legrain, J. M. Park, N. F. Q. Yuan, K. Watanabe, T. Taniguchi, R. M. Fernandes, L. Fu, and P. Jarillo-Herrero, Nematicity and competing orders in superconducting magic-angle graphene, Science **327**, 264 (2021).

⁵⁰ Y. Jiang, X. Lai, K. Watanabe, T. Taniguchi, K. Haule, J. Mao, and E. Y. Andrei, Charge-order and broken rotational symmetry in magic angle twisted bilayer graphene, Nature (London) **573**, 91 (2019).

⁵¹ H. Ji, Y. Liu, Y. Li, X. Ding, Z. Xie, C. Ji, S. Qi, X. Gao, M. Xu, P. Gao, L. Qiao, Y.-F. Yang, G.-M. Zhang, and J. Wang, Rotational symmetry breaking in superconducting nickelate $\text{Nd}_{0.8}\text{Sr}_{0.2}\text{NiO}_2$ films, Nat. Commun. **14**, 7155 (2017).

⁵² C. Eckberg, D. J. Campbell, T. Metz, J. Collini, H. Hodovanets, T. Drye, P. Zavalij, M. H. Christensen, R. M. Fernandes, S. Lee, P. Abbamonte, J. W. Lynn, and J. Paglione, Sixfold enhancement of superconductivity in a tunable electronic nematic system, Nat. Phys. **16**, 346 (2020).

⁵³ L. Dell'Anna and W. Metzner, Fermi surface fluctuations and single electron excitations near Pomeranchuk instability in two dimensions, Phys. Rev. B **73**, 045127 (2006).

⁵⁴ J. Rech, C. Pépin, A. V. Chubukov, Quantum critical behavior in itinerant electron systems: Eliashberg theory and instability of a ferromagnetic quantum critical point, Phys. Rev. B **74**, 195126 (2006).

⁵⁵ M. A. Metlitski and S. Sachdev, Quantum phase transitions of metals in two spatial dimensions. I. Ising-nematic order, Phys. Rev. B **82**, 075127 (2010).

⁵⁶ H. Yamase and R. Zeyher, Superconductivity from orbital nematic fluctuations, Phys. Rev. B **88**, 180502(R) (2013).

⁵⁷ T. Maier and D. J. Scalapino, Pair structure and the pair-

ing interaction in a bilayer Hubbard model for unconventional superconductivity, *Phys. Rev. B* **90**, 174510 (2014).

⁵⁸ S. Lederer, Y. Schattner, E. Berg, S. Kivelson, Enhancement of Superconductivity near a Nematic Quantum Critical Point, *Phys. Rev. Lett.* **114**, 097001 (2015).

⁵⁹ M. A. Metlitski, D. F. Mross, S. Sachdev, and T. Senthil, Cooper pairing in non-Fermi liquids, *Phys. Rev. B* **91**, 115111 (2015).

⁶⁰ M. Einenkel, H. Meier, C. Pépin, and K. B. Efetov, Pairing gaps near ferromagnetic quantum critical points, *Phys. Rev. B* **91**, 064507 (2015).

⁶¹ S. Raghu, G. Torroba, and H. Wang, Metallic quantum critical points with finite BCS couplings, *Phys. Rev. B* **92**, 205104 (2015).

⁶² Y. Wang, A. Abanov, B. L. Altshuler, E. A. Yuzbashyan, and A. V. Chubukov, Superconductivity near a quantum-critical point: The special role of the first Matsubara frequency, *Phys. Rev. Lett.* **117**, 157001 (2016).

⁶³ Y. Schattner, S. Lederer, S. Kivelson, and E. Berg, Enhancement of Superconductivity near a Nematic Quantum Critical Point, *Phys. Rev. X* **6**, 031028 (2016).

⁶⁴ S. Lederer, Y. Schattner, E. Berg, and S. Kivelson, Superconductivity and non-Fermi liquid behavior near a nematic quantum critical point, *Proc. Natl. Acad. Sci. U.S.A.* **114**, 4905 (2017).

⁶⁵ T. Agatsuma and H. Yamase, Structure of the pairing gap from orbital nematic fluctuations, *Phys. Rev. B* **94**, 214505 (2016).

⁶⁶ H. Wang, Y. Wang, and G. Torroba, Superconductivity versus quantum criticality: Effects of thermal fluctuations, *Phys. Rev. B* **97**, 054502 (2018).

⁶⁷ P. T. Dumitrescu, M. Serbyn, R. T. Scalettar, and A. Vishwanath, Superconductivity and nematic fluctuations in a model of doped FeSe monolayers: Determinant quantum Monte Carlo study, *Phys. Rev. B* **94**, 155127 (2016).

⁶⁸ A. Klein and A. V. Chubukov, Superconductivity near a nematic quantum critical point: Interplay between hot and lukewarm regions, *Phys. Rev. B* **98**, 220501(R) (2018).

⁶⁹ A. Klein, Y.-M. Wu, and A. V. Chubukov, Multiple intertwined pairing states and temperature-sensitive gap anisotropy for superconductivity at a nematic quantum-critical point, *npj Quantum Materials* **4**, 55 (2019).

⁷⁰ Y.-M. Wu, A. Abanov, Y. Wang, and A. V. Chubukov, Special role of the first Matsubara frequency for superconductivity near a quantum critical point: Nonlinear gap equation below T_c and spectral properties in real frequencies, *Phys. Rev. B* **99**, 144512 (2019).

⁷¹ J. A. Damia, S. Kachru, S. Raghu, and G. Torroba, Two-dimensional non-Fermi-liquid metals: A solvable large-N limit, *Phys. Rev. Lett.* **123**, 096402 (2019).

⁷² A. Klein, A. V. Chubukov, Y. Schattner, and E. Berg, Normal State Properties of Quantum Critical Metals at Finite Temperature, *Phys. Rev. X* **10**, 031053 (2020).

⁷³ J. Aguilera Damia, M. Solis, and G. Torroba, How non-Fermi liquids cure their infrared divergences, *Phys. Rev. B* **102**, 045147 (2020).

⁷⁴ J. Aguilera Damia, M. Solis, and G. Torroba, Thermal effects in non-Fermi liquid superconductivity, *Phys. Rev. B* **103**, 155161 (2021).

⁷⁵ A. Migdal, Interaction between electrons and lattice vibrations in a normal metal, *Sov. Phys. JETP* **7**, 996 (1958).

⁷⁶ G. M. Eliashberg, Interaction between electrons and lattice vibrations in a superconductor, *Sov. Phys. JETP* **11**, 696 (1960).

⁷⁷ S.-S. Zhang, Z. M. Raines, and A. V. Chubukov, Applicability of Eliashberg theory for systems with electron-phonon and electron-electron interaction: A comparative analysis, *Phys. Rev. B* **109**, 245132 (2024).

⁷⁸ Y. Nambu, Quasi-particles and gauge invariance in the theory of superconductivity, *Phys. Rev.* **117**, 648 (1960).

⁷⁹ P. B. Allen and B. Mitrović, *Theory of Superconducting T_c* , Solid State Physics, Vol.37 (Academic Press, Inc., 1982).

⁸⁰ J. P. Carbotte, Properties of boson-exchange superconductors, *Rev. Mod. Phys.* **62**, 1027 (1990).

⁸¹ F. Marsiglio, Eliashberg theory: A short review, *Ann. Phys.* **417**, 168102 (2020).

⁸² D. Hauck, M. J. Klug, I. Esterlis, and J. Schmalian, Eliashberg equations for an electron-phonon version of the Sachdev-Ye-Kitaev model: Pair breaking in non-Fermi liquid superconductors, *Ann. Phys.* **417**, 168120 (2020).

⁸³ A. V. Chubukov, A. Abanov, Y. Wang, and Y.-M. Wu, The interplay between superconductivity and non-Fermi liquid at a quantum-critical point in a metal, *Ann. Phys.* **417**, 168142 (2020).

⁸⁴ I. Esterlis and J. Schmalian, Quantum critical Eliashberg theory, arXiv:2506.11952.

⁸⁵ I. Esterlis, B. Nosarzewski, E. W. Huang, B. Moritz, T. P. Devoreaux, D. J. Scalapino, and S. A. Kivelson, Breakdown of the Migdal-Eliashberg theory: A determinant quantum Monte Carlo study, *Phys. Rev. B* **97**, 140501(R) (2018).

⁸⁶ M. N. Gastiasoro, J. Ruhman, and R. M. Fernandes, Superconductivity in dilute SrTiO₃: A review, *Ann. Phys.* **417**, 168107 (2020).

⁸⁷ F. Schrödi, P. M. Oppeneer, and A. Aperis, Unconventional superconductivity mediated solely by isotropic electron-phonon interaction, *Phys. Rev. B* **102**, 024503 (2020).

⁸⁸ S. B. Mishra, H. Mori, and E. R. Margine, Electron-phonon vertex correction effect in superconducting H₃S, arXiv:2507.01897v1.

⁸⁹ M. Franz, Z. Tešanović, and O. Vafek, QED₃ theory of pairing pseudogap in cuprates: From *d*-wave superconductor to antiferromagnet via an algebraic Fermi liquid, *Phys. Rev. B* **66**, 054535 (2002).

⁹⁰ D. M. Mross, J. McGreevy, H. Liu, and T. Senthil, Controlled expansion for certain non-Fermi-liquid metals, *Phys. Rev. B* **82**, 045121 (2010).

⁹¹ S. C. Thier and W. Metzner, Singular order parameter interaction at the nematic quantum critical point in two-dimensional electron systems, *Phys. Rev. B* **84**, 155133 (2011).

⁹² G. Torroba and H. Wang, Quantum critical metals in $4-\epsilon$ dimensions, *Phys. Rev. B* **90**, 165144 (2014).

⁹³ H. Wang and G. Torroba, Non-Fermi liquids at finite temperature: Normal-state and infrared singularities, *Phys. Rev. B* **96**, 144508 (2017).

⁹⁴ T. Holder and W. Metzner, Non-Fermi-liquid behavior at the onset of incommensurate $2k_F$ charge- or spin-density wave order in two dimensions, *Phys. Rev. B* **90**, 016106(R) (2014).

⁹⁵ L. Debbeler and W. Metzner, Non-Fermi liquid behavior at flat hot spots from quantum critical fluctuations at the onset of charge- or spin-density wave order, *Phys. Rev. B* **107**, 165152 (2023).

⁹⁶ L. Debbeler and W. Metzner, Marginal Fermi liquid behavior at the onset of $2k_F$ density wave order in two-dimensional metals with flat hot spots, *Phys. Rev. B* **109**, 235112 (2024).

⁹⁷ T. Grover and J. McGreevy, A critical theory for solidification of a liquid Fermi liquid, arXiv:2504.06508.

⁹⁸ G.-Z. Liu, Z.-K. Yang, X.-Y. Pan, and J.-R. Wang, Towards exact solutions for the superconducting T_c induced by electron-phonon interaction. *Phys. Rev. B* **103**, 094501 (2021).

⁹⁹ P. K. Nag, K. Scott, V. S. de Carvalho, J. K. Byland, X. Yang, M. Walker, A. G. Greenberg, P. Klavins, E. Miranda, A. Gozar, V. Taufour, R. M. Fernandes, and E. H. da Silva Neto, Highly anisotropic superconducting gap near the nematic quantum critical point of $\text{FeSe}_{1-x}\text{S}_x$. *Nat. Phys.* **21**, 89 (2025).

¹⁰⁰ P. J. Davis, *Interpolation and Approximation*, Chap. 2.2 (Blaisdell, New York, 1963).

¹⁰¹ I. Paul and M. Garst, Lattice effects on nematic quantum criticality in metals. *Phys. Rev. Lett.* **118**, 227601 (2017).

¹⁰² D. Labat and I. Paul, Pairing instability near a lattice-influenced nematic quantum critical point, *Phys. Rev. B* **96**, 195146 (2017).

¹⁰³ V. S. de Carvalho and H. Freire, Superconductivity near a nematic quantum critical point, *Phys. Rev. B* **105**, L220501 (2022).

¹⁰⁴ M. H. Christensen, M. Schuett, A. Klein, and R. M. Fernandes, Microscopic origin of the nematic-elastic coupling and dynamics of hybridized collective nematic-phonon excitations. arXiv:2507.03546v1.

¹⁰⁵ X. Chen, S. Maiti, R. M. Fernandes, and P. J. Hirschfeld, Nematicity and superconductivity: Competition versus cooperation, *Phys. Rev. B* **102**, 184512 (2020).

¹⁰⁶ J. Kang, A. V. Chubukov, and R. M. Fernandes, Time-reversal symmetry-breaking nematic superconductivity in FeSe, *Phys. Rev. B* **98**, 064508 (2018).

¹⁰⁷ K. R. Islam and A. Chubukov, Unconventional superconductivity mediated by nematic fluctuations in a multiorbital system: Application to doped FeSe, *Phys. Rev. B* **111**, 094503 (2025).